Turbulent premixed combustion in the laminar flamelet and the thin reaction zone regime

By H. Wenzel[1]

1. Motivations and objectives

1.1 Definition of the thin reaction zone regime

Turbulent premixed combustion is a complex and important process in many engineering applications. The two-way coupling between the turbulent flow and the chemical kinetics produces an intractable problem in its entirety, and simplifications to either the fluid dynamical or chemical components must be made.

Simplifications to the turbulent premixed combustion problems can be made by restricting the conditions under which flames are studied. One method of classifying premixed flame is demonstrated by the plot in Fig. 1. Here the flame is categorized according to two ratios of turbulent flow and flame scales: (1) the velocity ratio u'/s_L, where u' is the root mean square velocity fluctuation and s_L is the laminar burning velocity, and (2) ℓ/ℓ_F, where ℓ is the integral length scale of the turbulence and ℓ_F is the flame thickness. We can subdivide this domain into several regimes. For values of $u'/s_L < 1$ one speaks of the wrinkled flame regime. As the turbulence intensity increases, flames enter the corrugated flame regime. This regime exists as one increases turbulence intensity until the Karlovitz number, defined as

$$\mathrm{Ka} = t_F/t_\eta = \ell_F^2/\eta^2 \ , \tag{1}$$

reaches unity. The Karlovitz number is the ratio of the flame to Kolmogorov time scales, where $t_F = \ell_F/s_L$, and the Kolmogorov length and times scales are $\eta = (\nu^3/\epsilon)^{1/4}$ and $t_\eta = (\nu/\epsilon)^{1/4}$. As seen in Eq. 1, unity Ka also implies unity $\ell_F/\eta = 1$ (for cases with unity Schmidt number $\mathrm{Sc} = 1$).

One can also define a Karlovitz number in terms of the reaction zone thickness. This is advantageous when one considers large activation energy asymptotics (e.g. Peters 1992a), where the flame structure of a one-step chemical mechanism consists of a chemically inert preheat zone and a reaction zone, (Fig. 2). The thickness of the reaction zone δ is typically one order of magnitude smaller than the preheat zone. This gives rise to the definition of a Karlovitz number based on the reaction zone thickness:

$$\mathrm{Ka}_\delta = \delta^2/\eta^2 = \mathrm{Ka}\,\delta^2/\ell_F^2 \ . \tag{2}$$

From this expression, one can derive relations between the turbulence intensity u'/s_L and the length scale ratio ℓ/ℓ_F, again under the assumption of $\mathrm{Sc} = 1$:

$$u'/s_L = \mathrm{Re}\,(\ell/\ell_F)^{-1} = \mathrm{Ka}^{2/3}(\ell/\ell_F)^{1/3} \ . \tag{3}$$

1 Institut für Technische Mechanik, RWTH Aachen, Germany

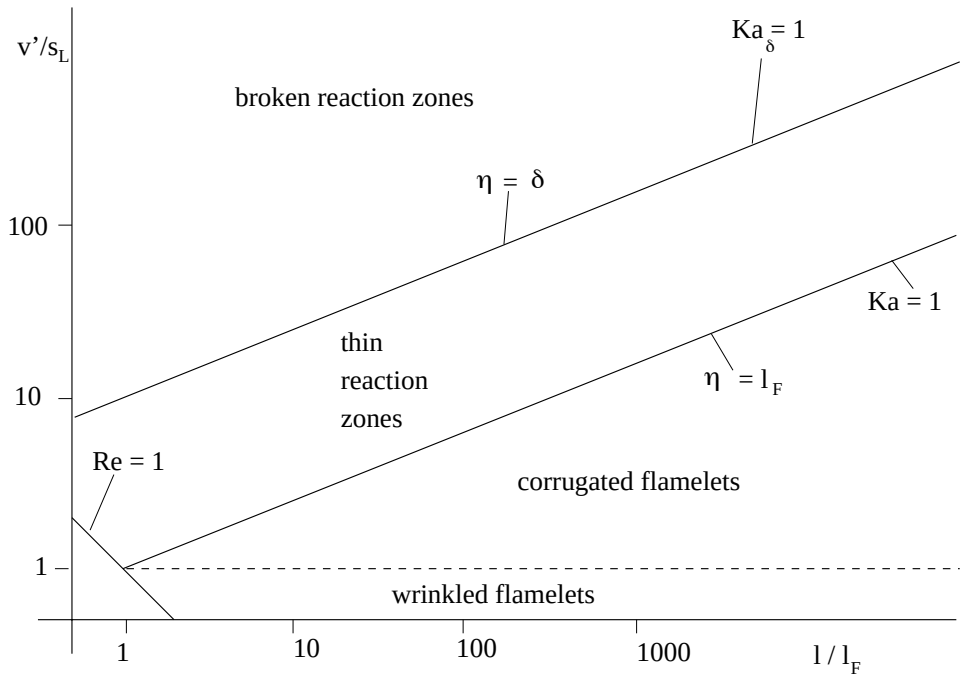

FIGURE 1. Regime diagram for premixed turbulent combustion.

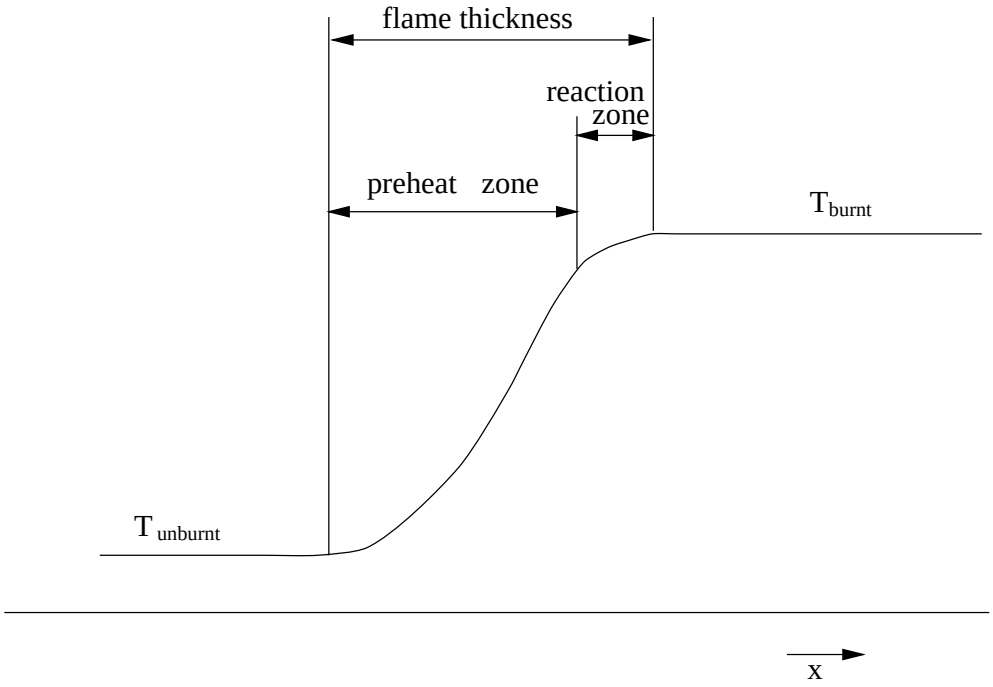

FIGURE 2. Asymptotic structure of a premixed laminar flame.

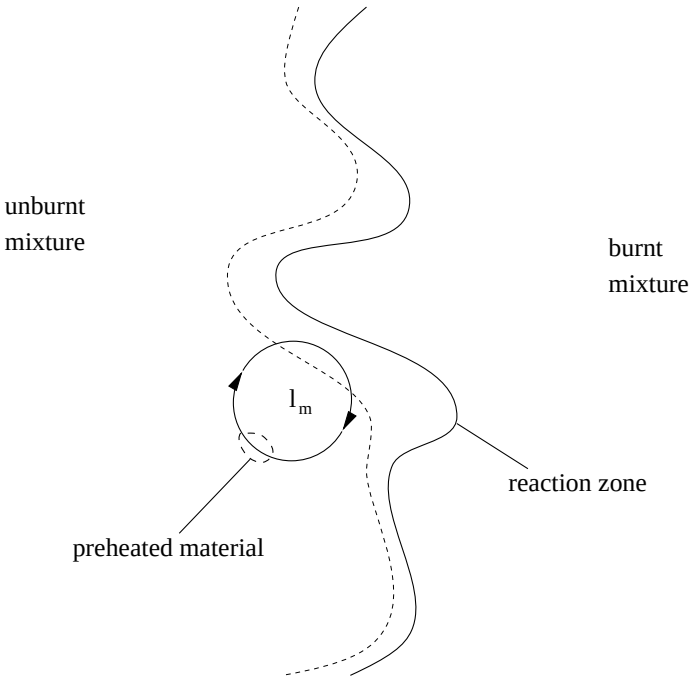

FIGURE 3. Interaction between an eddy of the size l_m and a turbulent flame front.

The line where $\mathrm{Ka}_\delta = 1$, or $\eta = \delta$, depicts the separation between the thin and broken reaction zones.

The broken reaction zone regime is not accessible with the methods to be used in this study, and the corrugated and wrinkled flamelet regimes have been examined earlier (Peters 1992b). Therefore, the focus of this work is turned to the only recently described thin reaction zone regime (Peters 1997). In this regime the Kolmogorov length is less than the flame thickness but larger than the reaction zone thickness, so that the smallest turbulent eddies may penetrate the preheat zone but not the reaction zone. The characteristic length scale for this regime is defined as the size of an eddy in the inertial range which has a turnover time t_m equal to the flame time t_F:

$$l_m = (\varepsilon t_F^3)^{1/2} \ , \tag{4}$$

where ε is the turbulent dissipation u'^3/ℓ. If one interprets the flame time as the time needed to diffuse heat or chemical species over the flame thickness, $t_F = l_F^2/D$, then the physical meaning of l_m becomes clear as the maximum distance that preheated fluid can be transported away from the reaction zone by turbulent eddies, as illustrated in Fig. 3.

1.2 Derivation of a G-equation for the thin reaction zone regime

In the following, an equation for the displacement of the reaction zone is derived which is very similar to the G-equation for the flamelet regime. Because the turbulence now controls mixing in the preheat zone, the propagation velocity is no longer determined by the mixture alone, but by diffusion and transport effects within the preheat zone as well. We take a similar approach to Ruetsch & Broadwell 1995 and

Vervisch 1995, and start from a diffusive-reactive equation for the deficient species of a one-step chemical reaction:

$$\rho \left(\frac{\partial Y}{\partial t} + \mathbf{v} \cdot \nabla Y \right) = \nabla \cdot (\rho D \nabla Y) + \dot{\omega} \ . \tag{5}$$

Here Y is the mass fraction, $\mathbf{v}$ the fluid velocity, ρ the density, and $\dot{\omega}$ the chemical source term. We can define an isoscalar surface $Y(\mathbf{x}, t) = Y_0$ that marks the instantaneous position of the reaction zone. Its substantial derivative, $\mathrm{D}Y/\mathrm{D}t|_{Y=Y_0}$, vanishes everywhere and it therefore satisfies the equation:

$$\frac{\partial Y}{\partial t} + \nabla Y \cdot \left. \frac{\mathrm{d}\mathbf{x}}{\mathrm{d}t} \right|_{Y=Y_0} = 0 \ . \tag{6}$$

The normal vector on this isosurface which points into the unburnt region, $\mathbf{n} = \nabla Y/|\nabla Y|$, can be used to combine Eqs. 5 and 6 to derive an expression for the displacement speed of the reaction zone:

$$\left. \frac{d\mathbf{x}}{dt} \right|_{Y=Y_0} = \mathbf{v} - \left[\frac{\nabla \cdot (\rho D \nabla Y) + \dot{\omega}}{\rho |\nabla Y|} \right] \mathbf{n} \ . \tag{7}$$

We now want to make the formal connection with the G equation derived by Kerstein *et al.* 1988. We introduce a scalar G so that the isosurface $G = G_0$ is identical to the isosurface $Y = Y_0$ and $G < G_0$ corresponds to the unburnt region. A similar equation to Eq. 6 can be written in terms of G:

$$\frac{\partial G}{\partial t} + \nabla G \cdot \left. \frac{\mathrm{d}\mathbf{x}}{\mathrm{d}t} \right|_{G=G_0} = 0 \ . \tag{8}$$

Eq. 7 may be introduced into Eq. 8 if we realize that the displacement speed and the normal vector are identical for both fields:

$$\frac{\partial G}{\partial t} + \mathbf{v} \cdot \nabla G = - \left[\frac{\nabla \cdot (\rho D \nabla Y) + \dot{\omega}}{\rho |\nabla Y|} \right] |\nabla G| \ , \tag{9}$$

The diffusive term on the right hand side can be split into a curvature term and a term representing diffusion along the normal:

$$\frac{\partial G}{\partial t} + \mathbf{v} \cdot \nabla G = -D \, \kappa |\nabla G| - \left[\frac{\mathbf{n} \cdot \nabla (\rho D \, \mathbf{n} \cdot \nabla Y) + \dot{\omega}}{\rho |\nabla Y|} \right] |\nabla G| \ . \tag{10}$$

where κ denotes the curvature $\kappa = \nabla \cdot \mathbf{n}$ and the normal vector is now given by the G field, $\mathbf{n} = -\nabla G/|\nabla G|$.

The expression in square brackets has the dimension of a velocity. In a steady, laminar, unstrained, planar flame it would be equal to the laminar burning velocity s_L^0, but here the propagation speed of the thin reaction zone can no longer be

prescribed due to the dependence on fluctuating quantities in the preheat zone upstream. It is reasonable, however, to expect it to be of the same order of magnitude as s_L^0. If this hypothesis holds, normalizing Eq. 10 with the Kolmogorov length and time scale shows each term of the order of unity, except for the last one, which is of the order of Ka^{-2} and therefore small in the thin reaction zone regime (Peters 1997). This assumption is supported by an earlier direct numerical simulation of the G-equation (Wenzel & Peters 1997). These simulations contained a laminar burning velocity that depended linearly on strain and curvature and showed a similar behavior of the eikonal propagation term becoming less important when the thin reaction zone regime is reached. In order to analyze Eq. 10, we use the statistical mean value for the expression in the square brackets, which is called $-s_L^*$, and the model G-equation for the thin reaction zone regime can be written:

$$\frac{\partial G}{\partial t} + \mathbf{v} \cdot \nabla G = -D\,\kappa |\nabla G| + s_L^* |\nabla G| \,. \tag{11}$$

The similarity to the G-equation for the laminar flamelet regime becomes apparent when we present the equation we are going to use for the direct numerical simulations in that regime:

$$\frac{\partial G}{\partial t} + \mathbf{v} \cdot \nabla G = -D_{\mathcal{L}}\,\kappa |\nabla G| + s_L^0 |\nabla G| \,, \tag{12}$$

where $D_{\mathcal{L}} = s_L^0 \mathcal{L}$ is the Markstein diffusivity taken with the Markstein length $\mathcal{L}$. This equation comes from an asymptotic analysis of the response of the flame speed on curvature and stretch (Clavin & Williams 1982) where the influence of the stretch has been neglected.

Both Eqs. 11 and 12 show exactly the same structure; the only differences are the replacement of the Markstein diffusivity $D_{\mathcal{L}}$ by the mass diffusivity D and the laminar burning velocity s_L^0, which is determined only through chemistry, by the propagation velocity of the reaction layer s_L^*, which is influenced by an interaction between the chemistry and the flow field. Another distinction between these equations should be noted. In the laminar flamelet regime the propagation term $s_L^0 |\nabla G|$ plays the most prominent role, whereas in the thin reaction zone regime the evolution of G is primarily influenced by the curvature term $-D\,\kappa |\nabla G|$

1.3 The equation for $\overline{|\nabla G|}$ for the laminar flamelet and the thin reaction zone regime

In modeling turbulent premixed combustion the determination of the ratio of the turbulent to the laminar burning velocity plays an important role. Kerstein *et al.* 1988 could show that this quantity is, under some restrictions, equal to the absolute value of the gradient of G, which is called $\overline{\sigma} \equiv \overline{|\nabla G|}$ in the subsequent part of this work.

Although an exact formulation for $\overline{\sigma}$ can be derived directly from Eqs. 11 and 12 by applying the operator $-(\mathbf{n} \cdot \nabla)$ and then averaging (Wenzel & Peters 1997,

Keller 1996), the resultant expression is intractable, and therefore a model equation for $\overline{\sigma}$ which is valid for both regimes was proposed by Peters 1997:

$$\frac{\partial\overline{\sigma}}{\partial t}+\overline{\mathbf{v}}\cdot\nabla\overline{\sigma}=-D_t\overline{\kappa}(\overline{\sigma})|\nabla\overline{\sigma}|+c_0\frac{-\overline{v'_\alpha v'_\beta}}{\overline{k}}\frac{\partial\overline{v_\alpha}}{\partial x_\beta}\overline{\sigma}+c_1\frac{D_t(\nabla\overline{G})^2}{\overline{G'^2}}\overline{\sigma}-c_2\frac{s_L^0\overline{\sigma}^2}{\overline{G'^2}^{1/2}}-c_3\frac{D\overline{\sigma}^3}{\overline{G'^2}}\ . \tag{13}$$

The terms on the left-hand side are the unsteady change and the convection of the mean value, the first term on the right-hand side is the turbulent transport, the second the production by mean velocity gradients, and the third the production by turbulent fluctuations of the velocity field. The remaining two terms are sink terms; the one proportional to $\overline{\sigma}^2$ due to flame propagation is of most importance in the flamelet regime. The last one comes from the curvature term in the G-equation and is most active in the thin reaction zone regime. For a further details regarding this equation the readers are referred to Peters (1997).

In the following sections of this study we will carry out a direct numerical simulation for turbulent premixed combustion both in the laminar flamelet and in the thin reaction zone regime by solving Eqs. 11 and 12 numerically for the case of homogeneous, isotropic turbulence. The objective is to gain insight into the physical interaction of a propagating scalar with the flow field and to check the assumptions that had to be made in the process of deriving the equation for the mean value of σ, Eq. 13. Furthermore, we want to determine the model constants that appear in that equation.

This aim puts some severe demands on the numerical scheme to be used: (1) it has to be highly accurate to avoid numerical diffusion contaminating the solution, and (2) it has to be stable for a wide range of the two parameters: the burning velocity and diffusivity. The first goal was achieved by using a pseudo-spectral code. To accomplish the second goal a new numerical scheme had to be developed that allows for the formation of cusps in a iso-G front.

2. Accomplishments

As mentioned above, we want to solve the G-equation subjected to homogeneous, isotropic turbulence. The underlying turbulent flow field was calculated using a pseudo-spectral code developed and described in Ruetsch 1992. This code is able to compute the development of a dissipative scalar in addition to the flow field. This feature was used to solve the complete left-hand side of the G-equation and the diffusive term on the right-hand side. The main part of the following section focuses on the incorporation of the eikonal propagation term $s_L|\nabla G|$ into the computer code and the evaluation of the numerical scheme by comparing it to an analytical solution of the G-equation.

2.1 A numerical scheme for the G-equation

To make the following part as clear as possible, we turn attention now solely towards the propagation term of the G-equation; convection and diffusion are not taken into account. The equation we want to solve then is:

$$\frac{\partial G}{\partial t}=s_L|\nabla G|\ , \tag{14}$$

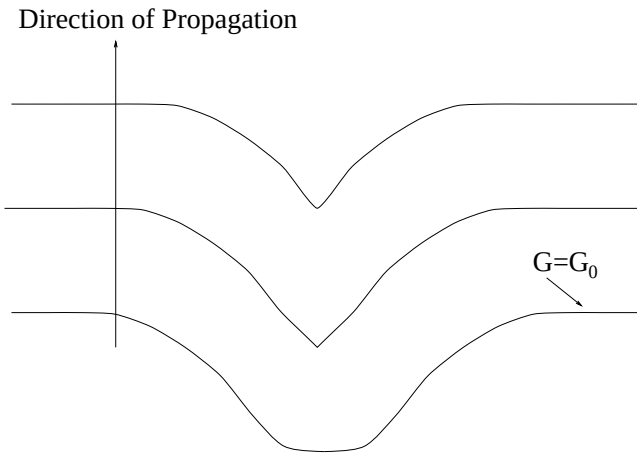

FIGURE 4. Formation of cusps.

where s_L is a prescribed constant propagation velocity.

It is well known (e.g. Kerstein *et al.* 1988, Sethian 1996) that this equation governs the motion of a front due to Huygen's principle through a quiescent medium. One feature of this type of propagation is the formation of cusps from an initially smooth front. This is illustrated in Fig. 4. At the location of these cusps, the derivative of G undergoes a jump, which makes the numerical treatment of Eq. 14 quite difficult. Some previous studies (e.g. Im *et al.* 1996) therefore tried to suppress the formation of cusps by choosing the diffusivity in the G-equation (Eqs. 11 and 12) large enough so the sharp gradients did not occur. This way of circumventing this difficulty is no longer applicable if we want to analyze these equations in the zero diffusivity limit.

We will use a numerical scheme that was originally developed for a scalar hyperbolic conservation law and was applied to this class of level-set equations by Sethian (1996). It has previously been used on this particular problem by Wenzel & Peters (1997) in the framework of a second-order finite-difference method.

To see the connection between the G-equation and a hyperbolic equation we rewrite Eq. 14 for the one dimensional case:

$$\frac{\partial G}{\partial t} - s_L|\nabla G| = \frac{\partial G}{\partial t} - s_L \frac{\partial G/\partial x}{|\partial G/\partial x|}\frac{\partial G}{\partial x} = \frac{\partial G}{\partial t} \pm s_L \frac{\partial G}{\partial x} = 0 \ . \tag{15}$$

This is actually a hyperbolic conservation equation for G with $\pm s_L$ as the signal velocity.

If we adopt this interpretation of the G-equation, we may use an upwind-scheme for the numerical calculation of this equation. To do so we follow the procedure outlined in Sethian (1996) and transform Eq. 15 again, into an equivalent Hamiltonian formulation:

$$\frac{\partial G}{\partial t} + H\left(\frac{\partial G}{\partial x}\right) = 0 \ , \tag{16}$$

with the Hamiltonian H defined as:

$$H\left(\frac{\partial G}{\partial x}\right) = -s_L \frac{\partial G/\partial x}{|\partial G/\partial x|}\frac{\partial G}{\partial x} \; . \tag{17}$$

A numerical approximation of this expression might be given in terms of derivatives of the G-field to the left and right of the point x_i where we want to compute the Hamiltonian:

$$H\left(\frac{\partial G}{\partial x}\right)\Big|_{x_i} \approx h(D^l G\big|_{x_i}, D^r G\big|_{x_i}) \; . \tag{18}$$

The numerical Hamiltonian $h(D^l G\big|_{x_i}, D^r G\big|_{x_i})$ is evaluated like the flux function of a Godunov Scheme for a scalar hyperbolic conservation law. Sethian (1996) uses the Enquist-Osher scheme in his work to calculate this quantity, but this scheme suffers from the implicit addition of diffusivity by replacing a compression shock by a compression wave in the corresponding Riemann problem. We therefore use an exact formulation that was given in Hirsch (1990):

$$h(D^l G\big|_{x_i}, D^r G\big|_{x_i}) = \begin{cases} min(H(D^l G\big|_{x_i}), H(D^r G\big|_{x_i})) & \text{if} \quad D^l G\big|_{x_i} \le D^r G\big|_{x_i} \\ max(H(D^l G\big|_{x_i}), H(D^r G\big|_{x_i})) & \text{if} \quad D^l G\big|_{x_i} > D^r G\big|_{x_i} \\ max(H(D^l G\big|_{x_i}), H(D^r G\big|_{x_i}), H(0)) & \text{if} \quad D^l G\big|_{x_i} > D^r G\big|_{x_i} \\ & \qquad \wedge \, D^l G\big|_{x_i} \cdot D^r G\big|_{x_i} < 0 \end{cases} \; . \tag{19}$$

Exact in this context means that in the Riemann problem all characteristics retain their nature and no shock is replaced by a fan or vice versa.

The evaluation of Eq. 19 needs the calculation of the spatial derivatives $D^{r/l}G|_{x_i}$ of the G-field. They are computed at points $x_{i\pm 1/2} = x_i \pm \Delta x/2$ using a spectral method.

The entire numerical procedure above could only be extended from a finite-difference framework to this pseudo-spectral framework because we followed a view on pseudo-spectral methods that Fornberg (1996) developed. He interprets them as a high-accuracy limit of finite-difference methods, so that the upwind scheme presented here becomes applicable.

To integrate these formulas into the computer code, they need an extension from one to three dimensions. This, fortunately, is quite straightforward. Either in the simplified G-equation Eq. 14 or in Eqs. 11 and 12, the eikonal term $s_L|\nabla G|$ can be computed by the sum of the numerical Hamiltonians h in the $x-$, $y-$, and $z-$directions:

$$s_L|\nabla G| \approx -\Big(h(D^l G\big|_{x_i}, D^r G\big|_{x_i}) + h(D^l G\big|_{y_i}, D^r G\big|_{y_i}) + h(D^l G\big|_{z_i}, D^r G\big|_{z_i})\Big) \; . \tag{20}$$

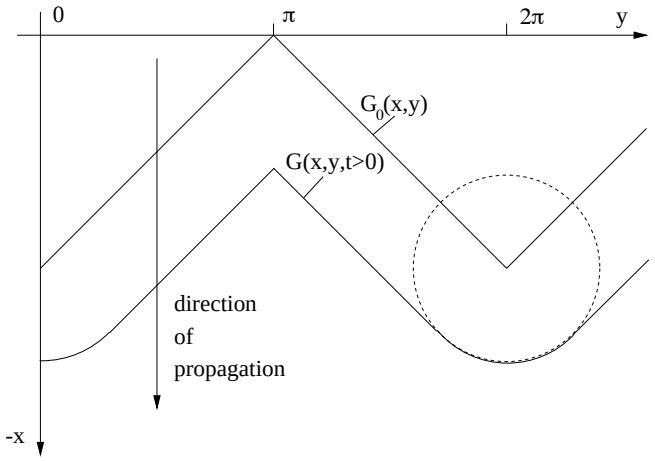

FIGURE 5. Propagation of an iso-G front according to the Huyghen's principle.

The three-dimensional Hamiltonian H which is needed in the evaluation of Eq. 20 is defined as:

$$H\left(\frac{\partial G}{\partial x_\alpha}\right) = -s_L \frac{\partial G/\partial x_\alpha}{\sqrt{(\partial G/\partial x_k)(\partial G/\partial x_k)}} \frac{\partial G}{\partial x_\alpha} \ , \tag{21}$$

where Einstein's summation convention is only applied to the index k and not to the index α.

2.2 Validation of the numerical scheme for the G-equation

Spectral methods are known to perform quite poorly when discontinuities are present in the solution (Canuto *et al.* 1988). For that reason the numerical scheme developed in this work needs to be validated. To that end we will construct an analytical solution for a two-dimensional version of Eq. 14 with a specific initial condition and check that against the numerical solution with the new scheme.

The derivation of the analytical solution is given first. On a 2π periodic grid, the G-field is initialized as a sawtooth function:

$$G_0(x,y) = \begin{cases} x - y & \text{for} \quad 0 \le y < \pi \\ x + y - 2\pi & \text{for} \quad \pi \le y < 2\pi \end{cases} \ . \tag{22}$$

Each iso-G front propagates according to the Huyghen's principle, as shown in Fig. 5. The solution for $G(x,y,t)$ can be constructed by geometrical considerations. Only the region $0 \le y < \pi$ is taken into account. The equation for the region $y \le \pi < 2\pi$ immediately follows from symmetry.

The general procedure is to divide the domain into a subdomain which is not influenced by the rarefaction fan that develops at the leading edge of the G-front, and a subdomain which is influenced by it. Within each subdomain the spatial derivatives can be formulated and and then fed into the two-dimensional G-equation, so that the time integration is possible. The outermost point influenced by the

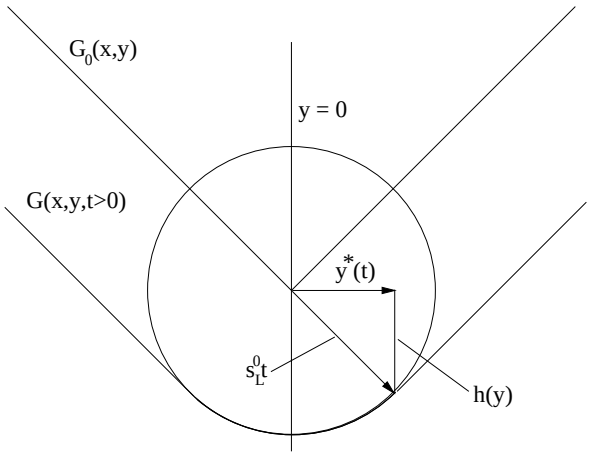

FIGURE 6. Detail of the the Huyghen's propagation.

rarefaction fan, y^*, travels in y-direction with a constant speed of $s_L/\sqrt{2}$, see Fig. 6. Inside the rarefaction fan the following relation holds:

$$h(y) = \sqrt{(s_L t)^2 - y^2} \Rightarrow \frac{\partial h}{\partial y} \equiv \frac{\partial G}{\partial y} = -\frac{y}{\sqrt{(s_L t)^2 - y^2}} \,. \tag{23}$$

Since all the spatial partial differentials in the G-equation are known, the time integration can be carried out:

$$\frac{\partial G}{\partial t} = s_L \sqrt{\frac{\partial G}{\partial x}^2 + \frac{\partial G}{\partial y}^2} = \begin{cases} s_L \sqrt{1 + \dfrac{y^2}{(s_L t)^2 - y^2}} & \text{for} \quad 0 \le y < \dfrac{s_L t}{\sqrt{2}} \\ s_L \sqrt{2} & \text{for} \quad \dfrac{s_L t}{\sqrt{2}} \le y < \pi \end{cases} \,. \tag{24}$$

Defining the time $t^* = \sqrt{2} y / s_L$, when the rarefaction fan reaches a point on the y-axis, one obtains the following analytical equation for $G(x, y, t)$:

$$G(x,y,t) = \begin{cases} G_0(x,y) + \sqrt{2} s_L t & \text{for} \quad t \le t^* \\ G(x,y,t^*) + s_L \displaystyle\int_{t^*}^{t} \sqrt{1 + \frac{y^2}{(s_L \tilde{t})^2 - y^2}} d\tilde{t} = & \text{for} \quad t > t^* \\ G_0(x,y) + 2y + \sqrt{(s_L t)^2 - y^2} - \sqrt{(s_L t^*)^2 - y^2} & \end{cases} \,. \tag{25}$$

The numerical solution for that problem has to capture the two basic features of a propagating scalar according to the Huyghen's principle (see Fig. 5): (1) the cusps at the back of the front must retain their shape, and (2) circular rarefaction waves must develop at the leading edge. To confirm the reproduction of these feature by the numerical solution, the results of both numerical integration of this problem and the analytical solution from Eq. 25 for two different grid resolutions are presented

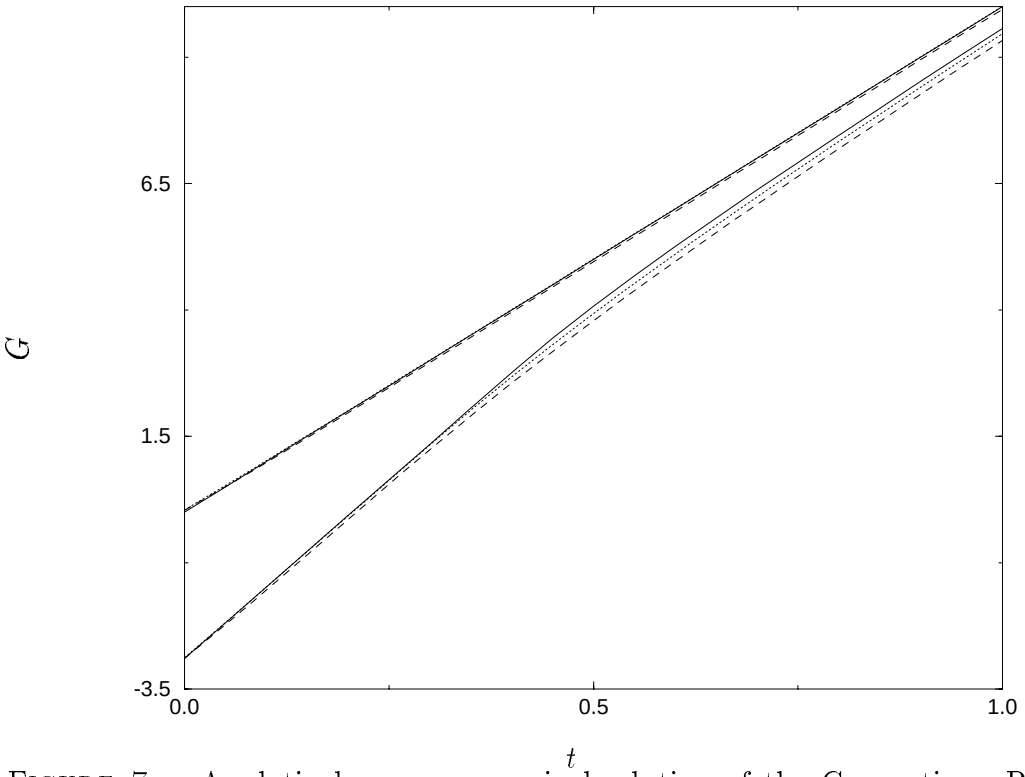

FIGURE 7. Analytical versus numerical solution of the G-equation. Results for two values of y are plotted. $y = 0$ corresponds to the upper set of lines, $y = 2.9$ to the lower set. ——— : analytical solution, - - - - : 32-point grid, ····· : 64-point grid.

in Fig. 7. This plot shows the time evolution for two points on the y-axis, $y = 0$ and $y = 2.9$. The first location was chosen because it is the leading edge of the propagating front, and any violation of feature (2) would become apparent. The ability of the scheme to capture feature (1) is proven with the time evolution at $y = 2.9$. This point lies very close to the the back of the front, and any problems in dealing with the cusp at that location should become apparent there.

The stability of the scheme is demonstrated in Fig 8 where the partial derivative $\partial G/\partial y$ for a typical case during the numerical calculation is shown. There are some overshoots in the vicinity of the cusp at $y = \pi$, but they are not amplified, and they actually become smaller because the jump in the derivatives gets smaller once the rarefaction fan reaches this position. Any disturbances introduced by the discontinuity in the gradient of G smooth out immediately by the variation-diminishing nature of the G-equation, if, in an explicit code, the CFL-condition formulated with the laminar burning velocity is obeyed.

The excellent agreement of the numerical scheme with the closed solution for this test case and its remarkable stability encourage its use in direct numerical simulations of the G-equation for turbulent flow.

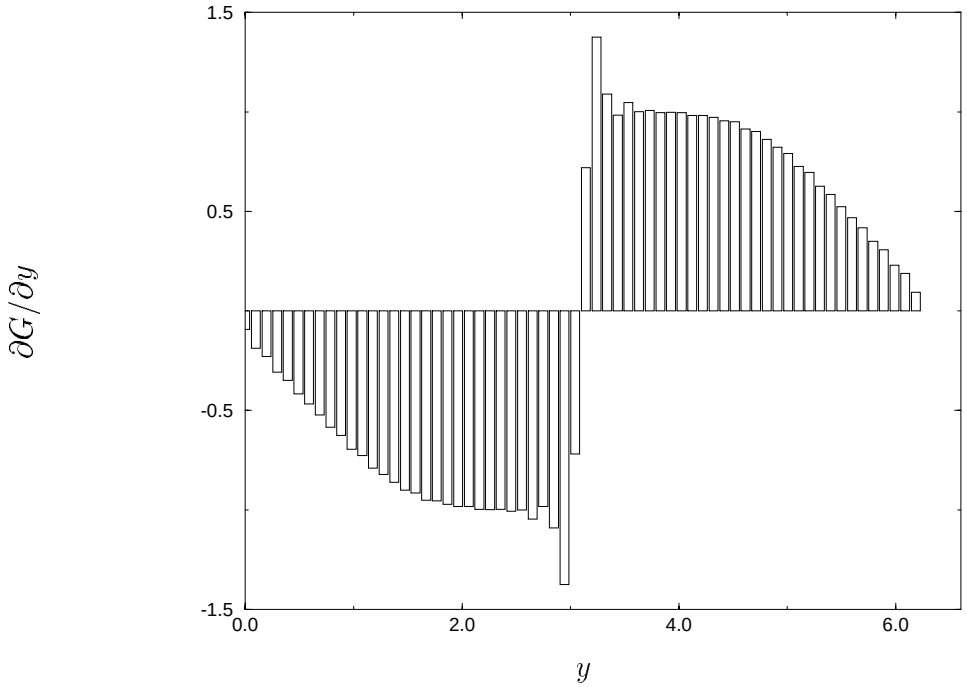

FIGURE 8. Partial y-derivative of the G-field at $t = 0.1755$.

2.3 The treatment of the curvature term $\kappa|\nabla G|$

The curvature term $\kappa|\nabla G|$ which appears in Eqs. 11 and 12 is basically diffusive in its nature and, therefore, much easier to incorporate into a pseudo-spectral code than the propagation term $s_L|\nabla G|$. However, it is highly nonlinear, and some caution has to be taken to minimize aliasing errors. To achieve this we express the curvature κ as:

$$\kappa = \nabla \cdot \mathbf{n} = \nabla \cdot \left(-\frac{\nabla G}{|\nabla G|} \right) = -\left(\frac{\nabla^2 G |\nabla G| - \nabla G \cdot \nabla |\nabla G|}{|\nabla G|^2} \right) \tag{26}$$

Using this relation, we can split $\kappa|\nabla G|$ into a linear diffusive term that can be treated very efficiently with a spectral method in Fourier space, and a nonlinear term:

$$-\kappa|\nabla G| = \nabla^2 G - \frac{\nabla G \cdot \nabla |\nabla G|}{|\nabla G|} = \nabla^2 G - \nabla G \cdot \nabla \ln(|\nabla G|) \; . \tag{27}$$

The nonlinear product $\nabla G \cdot \nabla \ln(|\nabla G|)$ is computed in physical space. It only contains a double product as opposed to a triple product that occurs in a direct evaluation of Eq. 24 and thus the aliasing error is much smaller.

2.4 Results

The DNS for Eqs. 11 and 12 were made on a 64^3-grid and statistical data was dumped every 50 time steps. Typical time series for $\overline{\sigma}$ are plotted in Fig. 9 for three different sets of the parameters burning velocity and diffusivity.

Saturation of $\overline{\sigma}$ was reached at approximately $t_0 = 0.85$. The computation was carried further until $t_1 = 2.5$; the difference is about 15 integral time scales of the

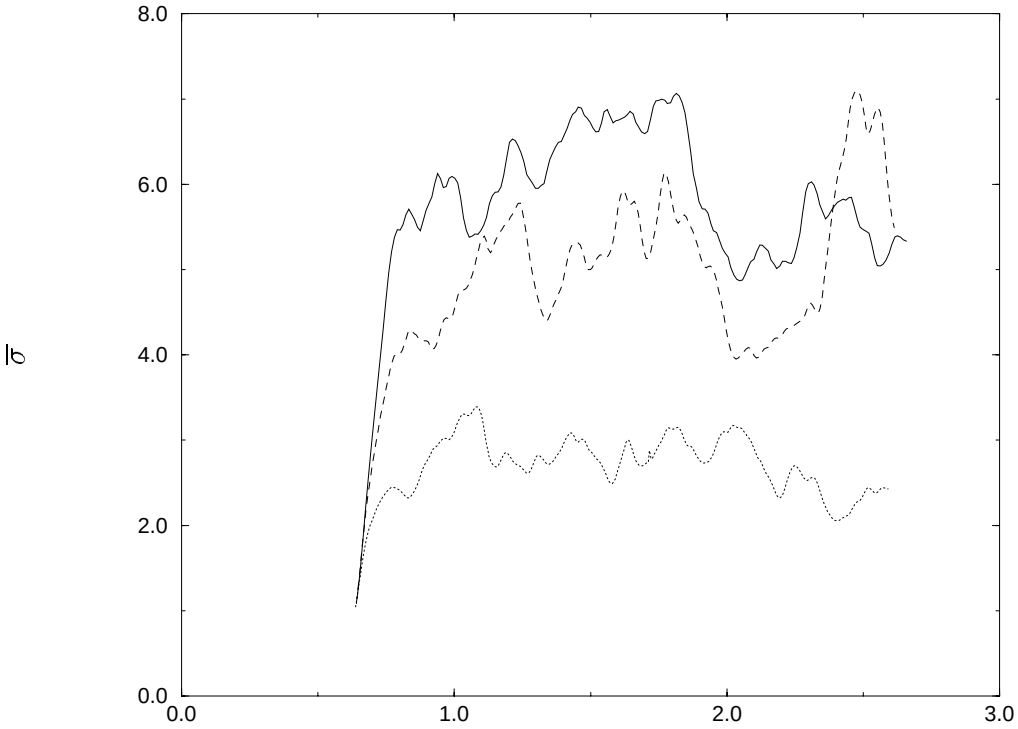

FIGURE 9. Time series of $\overline{\sigma}$. ——— : $s_L^0 = 1.0, D = 0.48$; - - - - : $s_L^0 = 8.0, D_{\mathcal{L}} = 0.0$; ····· : $s_L^0 = 16.0, D_{\mathcal{L}} = 0.0$.

flow, so that stable statistically stationary results can be expected. In that time interval the mean values of $\overline{\sigma}, u'$ and ℓ were time averaged. The results are given in the following table:

u'/s_L^0	ℓ/ℓ_F	$\overline{\sigma}$ (DNS-results)	$\overline{\sigma}$ (Eq. 28)
1.47	19.2	2.83	2.78
1.47	38.5	3.02	3.15
1.11	-	2.78	-
17.7	1.59	5.53	5.04
17.8	3.16	6.0	6.95
4.41	6.07	4.89	4.16
4.41	12.1	5.2	5.37
2.21	-	5.04	-
2.21	12.9	3.86	3.41
2.21	25.8	3.99	4.08

These results may be used to determine two of the constants in Eq. 13. After applying closure assumptions regarding the turbulent diffusivity, it is possible to derive an expression for $\overline{\sigma}$ in terms of the velocity ratio u'/s_L^0 and the length ratio ℓ/ℓ_F for the limit where the turbulent production of $\overline{\sigma}$ is balanced by the two

destruction terms in that equation (Peters 1997):

$$\overline{\sigma} = -\frac{0.39}{2}\frac{\ell}{\ell_F} + \sqrt{\left(\frac{0.39}{2}\frac{\ell}{\ell_F}\right)^2 + 0.78\,\alpha\,\frac{\ell}{\ell_F}\frac{u'}{s_L^0}}\,. \tag{28}$$

The implied assumption for the large scale turbulence limit $\overline{\sigma} = 2.0\,u'/s_L^0$ is fulfilled quite well in the runs with zero Markstein diffusivity. These are marked by a dash in the length ratio column in the table above since the flame thickness vanishes for that case. The constant $\alpha = c_3/c_1$ is then fitted with the results of the other DNS runs to a value of 1.3.

In this section we derived a new numerical scheme for solving the G-equation with a pseudo-spectral code. It was shown to possess the ability to handle the cusps that develop naturally in the propagation of a scalar due to Huyghen's principle. The direct numerical simulations that were carried out with this new scheme proved it to be a valuable tool in understanding premixed turbulent combustion because it can handle all possible sets of parameters that may appear if one analyzes this interesting and complex physical phenomenon in the framework of the G-equation.

3. Future work

In the near future we want to apply the code to gather more statistical data for the G-equation, the $\overline{\sigma}$-equation, and the equation for the variance of G. The latter equation was not presented in this work, but plays an important role in the closure of the turbulent G-equation if we don't retreat to the limiting case of production equals destruction in the model equation for $\overline{\sigma}$. It is then necessary to evaluate every term that appears in these equations, and the simple averaging procedure where the quantities are averaged over the whole box can no longer be used. Instead these quantities have to be conditionally averaged according to their position in the turbulent flame brush. This work was accomplished previously (Wenzel & Peters 1997) with finite-difference methods and has to be reimplemented using spectral methods.

In the formulation of dynamical sub-grid models for the G-equation there still lie some uncertainties (Im *et al.* 1996), which can be tackled using this newly developed numerical scheme because it can handle the interesting limiting case of zero diffusivity. In that context it will be of high interest to compute and compare the spectra of both the flow field and the scalar field. To get meaningful results from that kind of analysis, the resolution should be improved to a 96^3 or 128^3 grid to get a larger inertial range.

The whole study that was presented here dealt only with the passive G-equation. That is, heat release effects were not accounted for. By this heat release the flame can have influence back on the flow field, and some new interesting effects can be seen. In the future these phenomena should be definitively included in a direct numerical simulation of the turbulent G-equation, although it seems clear at this moment that a pseudo-spectral code can no longer be applied to solve that problem and some higher order finite-difference or finite-volume methods will have to be used.

Acknowledgments

I am grateful to Dr. G.R. Ruetsch for giving me the basic computer code, and for his help in learning to use it. I also want to thank him, Prof. J.H. Ferziger, and Dr. W.K. Bushe for valuable and enjoyable discussions.

REFERENCES

CANUTO, C., HUSSAINI, M.Y., QUARTERONI, A., & ZANG, T.A. 1988 *Spectral Methods in Fluid Dynamics.* Springer-Verlag.

CLAVIN, P. & WILLIAMS, F. 1982 Effects of molecular diffusion and of thermal expansion on the structure and dynamics of premixed flames in turbulent flows of large scale and low intensity. *J. Fluid Mech.* **116,** 251-282.

FORNBERG, B. 1996 *A practical guide to pseudo-spectral methods.* Cambridge Monographs on Applied and Computational Mathematics, Cambridge University Press.

HIRSCH, C. 1990 *Numerical Computation of internal and external flows Vol.2, chapter 20.5.1.* J. Wiley & Sons.

IM, H.G., LUND, T.S., & FERZIGER, J.H. 1996 Dynamic models for LES of turbulent front propagation with a spectral method. *Annual research briefs 1995*, Center for Turbulence Research, NASA Ames/Stanford Univ., 101-113.

KELLER, P. 1996 Berechnung der turbulenten Flammenausbreitung bei der ottomotorischen Verbrennung mit einem Flamelet-Modell. *Ph.D. Thesis.* RWTH Aachen.

KERSTEIN, A., ASHURST, W., & WILLIAMS, F. 1988 Field equation for interface propagation in an unsteady flow field. *Phys. Rev. A.* **37**(7), 2728-2731.

PETERS, N. 1992a Fifteen lectures on laminar and turbulent combustion: Lecture 6 *Ercoftac Summer School 1992.* RWTH Aachen.

PETERS, N. 1992b A spectral closure for premixed turbulent combustion in the flamelet regime. *J. Fluid Mech.* **242,** 611-629.

PETERS, N. 1997 The turbulent burning velocity for large scale and small scale turbulence. Submitted to: *J. Fluid Mech.*

RUETSCH, G.R. 1992 The structure and dynamics of the vorticity and passive scalar fields at small scales in homogeneous isotropic turbulence *Ph.D.Thesis.* Brown University.

RUETSCH, G.R. & BROADWELL, J.E. 1995 Effects of confinement on partially premixed flames. *Annual research briefs 1995*, Center for Turbulence Research, NASA Ames/Stanford Univ., 323-333.

SETHIAN, J.A 1996 A Review of the Theory, Algorithms, and Applications of Level Set Methods for Propagating Interfaces. *Acta Numerica.* Cambridge University Press.

VERVISCH, L. 1995 Probability density functions and dynamics of iso-concentration surfaces in premixed turbulent combustion.*Euroconference on Premixed Turbulent Combustion - Introduction to the State of the Art.* RWTH-Aachen.

WENZEL, H. & PETERS, N. 1997 Direct numerical simulation of premixed turbulent combustion using a flamelet approach. *Notes on Numerical Fluid Mechanics: Computation and Visualization of three-dimensional vortical and turbulent flows.* Viewer Verlag, to appear.